A Chandra Survey of Broad Absorption Line Quasars

THE ASTROPHYSICAL JOURNAL, 558:109–118, 2001 September 1

A *CHANDRA* SURVEY OF BROAD ABSORPTION LINE QUASARS

PAUL J. GREEN,[1] THOMAS L. ALDCROFT,[1] SMITA MATHUR,[2] BELINDA J. WILKES,[1] AND MARTIN ELVIS[1]

Received 2001 March 4; accepted 2001 May 15

ABSTRACT

We have carried out a survey with the *Chandra X-Ray Observatory* of a sample of 10 bright broad absorption line (BAL) quasars (QSOs). Eight of 10 sources are detected. The six brightest sources have only high-ionization BALs (hiBALs), while the four faintest all show low-ionization BALs (loBALs). We perform a combined spectral fit for hiBAL QSOs (384 counts total; 0.5–6 keV) to determine the mean spectral parameters of this sample. We derive an underlying best-fit power-law slope $\Gamma = 1.8 \pm 0.35$, which is consistent with the mean slope for radio-quiet QSOs from *ASCA*, but BAL QSOs require a (rest-frame) absorbing column of $6.5^{+4.5}_{-3.8} \times 10^{22}$ cm^{-2}, with a partial covering fraction of $\sim 80^{+9}_{-17}$%. The optical–to–X-ray spectral slope (α_{ox} from 2500 Å to 2 keV) varies from 1.7 to 2.4 across the full sample, consistent with previous results that BAL QSOs appear to be weak soft X-ray emitters. Removing the absorption component from our best-fit spectral model yields a range of α_{ox} from 1.55 to 2.28. All six hiBAL QSOs have deabsorbed X-ray emission consistent with non-BAL QSOs of similar luminosity. The spectral energy distributions of the hiBAL QSOs—both the underlying power-law slope and α_{ox}—provide the first conclusive evidence that BAL QSOs have appeared to be X-ray weak because of intrinsic absorption and that their underlying emission is consistent with non-BAL QSOs. By contrast, the removal of the best-fit absorption column detected in the hiBAL QSOs still leaves the four loBAL QSOs with values of $\alpha_{ox} > 2$ that are unusually X-ray faint for their optical luminosities, which is consistent with other evidence that loBALs have higher column density, dustier absorbers. Important questions of whether BAL QSOs represent a special line of sight toward a QSO nucleus or rather an early evolutionary or high-accretion phase in a QSO lifetime remain to be resolved, and the unique properties of loBAL QSOs will be an integral part of that investigation.

Subject headings: galaxies: active — quasars: emission lines — quasars: general — ultraviolet: galaxies — X-rays: galaxies

1. INTRODUCTION

While large surveys are rapidly increasing the number of known quasars (QSOs), our understanding of the QSO phenomenon grows more slowly. However, absorption lines caused by material intrinsic to the QSO hold great promise for revealing the conditions near the supermassive black holes that power them. The richest and most extreme absorption lines are found in quasars with broad absorption lines (BALs). About 10%–15% of optically selected QSOs have rest-frame ultraviolet spectra showing these BALs—deep absorption troughs displaced blueward from the corresponding emission lines in the high-ionization transitions of C IV, Si IV, N V, and O VI (high-ionization BALs [hiBALs]). About 10% of BAL QSOs also show broad absorption in lower ionization lines of Mg II or Al III (low-ionization BALs [loBALs]). BAL QSOs in general have higher optical/UV polarization than non-BAL QSOs, but the loBAL subsample tends to have particularly high polarization (Schmidt & Hines 1999) along with signs of reddening by dust (Sprayberry & Foltz 1992; Egami et al. 1996). All the BALs are commonly attributed to material along our line of sight flowing outward from the nucleus with velocities of 5000 up to $\sim$50,000 km s^{-1}. The observed ratios of broad emission and absorption line equivalent widths $W_\lambda^{em}/W_\lambda^{abs}$ and the detailed profiles of C IV BALs both imply that the covering factor of the BAL region must be less than 20% (Hamann, Korista, & Morris 1993). This observation, together with the similar fraction of QSOs showing BALs, suggests that most or possibly *all* QSOs contain BAL-type outflows. The optical/UV emission lines and continuum slopes of hiBAL QSOs are remarkably similar to those of non-BAL QSOs (Weymann et al. 1991). BAL QSOs may thus provide a unique probe of conditions near the nucleus of most QSOs. Ironically, although viewed from an obscured direction, BAL QSOs may nevertheless be particularly revealing.

In the last decade, a significant observational effort has been dedicated to BAL QSOs in the UV and X-ray bandpasses. The absorbing columns typically inferred from the UV spectra for the BAL clouds themselves (e.g., $N_H \sim 10^{20}$–10^{21} atoms cm^{-2}; Korista et al. 1992) appear low enough that we would a priori expect very little X-ray absorption ($\tau \ll 1$). It was initially a surprise then to discover that BAL QSOs are markedly underluminous in *soft* X-rays compared to their non-BAL QSO counterparts. Contrasting a complete sample of 36 BAL QSOs in the Large Bright Quasar Survey (LBQS) and the *ROSAT* All-Sky Survey (RASS) with carefully chosen comparison samples, Green et al. (1995) revealed definitively that BAL QSOs are *soft X-ray quiet as a class.* Deeper archival *ROSAT* Position Sensitive Proportional Counter (PSPC) pointings of 11 bona fide BAL QSOs confirmed this (Green & Mathur 1996, hereafter GM96), yielding unusually steep optical–to–X-ray slopes for BAL QSOs ($\alpha_{ox} \geq 1.9$[3]) relative

[1] Harvard-Smithsonian Center for Astrophysics, 60 Garden Street, Cambridge, MA 02138; pgreen@cfa.harvard.edu, aldcroft@cfa.harvard.edu, bwilkes@cfa.harvard.edu, melvis@cfa.harvard.edu.

[2] Department of Astronomy, Ohio State University, 140 West 18th Avenue, Columbus, OH 43210-1173; smita@astronomy.ohio-state.edu.

[3] The variable α_{ox} is the slope of a hypothetical power-law from 2500 Å to 2 keV; $\alpha_{ox} = 0.384 \log (L_{2500}/L_{2\,keV})$.

to non-BAL QSOs ($\alpha_{ox} \sim 1.6$) in the *ROSAT* bandpass. By *assuming* that the intrinsic (unabsorbed) spectral energy distributions (SEDs) of BAL QSOs are similar to those of non-BAL QSOs, GM96 found that absorbing columns of $N_H^{intr} \sim 10^{23}$ cm^{-2} are necessary to quench the X-ray flux to the observed (or upper limit) levels. Gallagher et al. (1999) studied a sample of eight BAL QSOs with *ASCA*, of which only two were detected. They estimated column densities of $\gtrsim 5 \times 10^{23}$ cm^{-2} to explain the nondetections, which are even higher than the *ROSAT* estimates. In some cases, the absorber is probably Compton-thick (i.e., $N_H^{intr} \gtrsim 10^{24}$ cm^{-2}), as in *ASCA* observations of PG 0946+301 (Mathur et al. 2000).

If the UV and X-ray absorption in quasars arises in the same region (see, e.g., Mathur et al. 1994), the large derived X-ray columns increase the best UV-derived estimates of both the ionization and mass outflow rate of BALs by 2–3 orders of magnitude. These highly ionized BAL outflows then represent a significant component of the QSO energy budget, but a single-zone photoionization model may not be appropriate, and other intriguing possibilities remain. BAL QSOs have been interpreted as normal QSOs seen along a line of sight either ablating off the edge of an obscuring torus or accelerated from the surface of the accretion disk in a wind (see, e.g., Murray & Chiang 1995; deKool & Begelman 1995; Elvis 2000). In this case, the inner wind-driven X-ray absorber shields the UV BAL clouds so that the UV BAL zone has a lower ionization than the X-ray absorber.

Even if the X-ray and UV absorbers are identical, the geometry, covering factor, temperature, density, metallicity, and ionization parameter of the absorbing clouds are poorly constrained from UV absorption line studies alone. The few absorption lines observed provide little if any constraint on the ionization of the absorbing material, leading to the simplifying assumption that the observed ions are the dominant species. Furthermore, BALs in the UV are often saturated (Wang et al. 1999), and column densities derived from UV measurements may also be significantly underestimated because of partial covering of the continuum source (Hamann 1998; Arav et al. 1999). Higher ionization absorbers are indicated not just by the X-ray absorption but by the detection of UV absorption in Ne VIII, O VI, and Si XII (Telfer et al. 1998). UV spectropolarimetry implies columns consistent with X-ray results (Goodrich 1997)—the most common UV BALs are saturated but partially filled in with scattered light.

Many results support the picture that BAL QSOs are *intrinsically normal* QSOs, with the BAL region an important part of every QSO's structure. Suggestive links between low-ionization BAL QSOs and IR-luminous mergers (Fabian 1999) and similarities between BAL QSOs and narrow-line Seyfert 1 galaxies (Mathur 2000; Brandt & Gallagher 2000) may also support a scenario where BAL QSOs are adolescent quasars in a transition phase, evolving from active high L/L_{Edd} (high Eddington fraction) to normal QSOs. If the BAL phase represents a high accretion rate period in a quasar's lifetime, then an intrinsic power law steeper than that for non-BAL QSOs might be expected, by analogy to narrow-line Seyfert galaxies and Galactic black hole candidate binary systems in outburst (Leighly 1999; Pounds, Done, & Osborne 1995).

Are the intrinsic SEDs of BAL QSOs really the same as non-BAL QSOs? X-ray spectroscopy can confirm the absorption interpretation and verify whether the underlying (unabsorbed) emission supports the hypothesis that BAL QSOs are typical QSOs seen from a privileged line of sight or rather a different phase or species of QSO. Unfortunately, because of low observed fluxes, there is only the following handful of BAL QSOs with X-ray spectroscopy:

1. In a 100 ks *ASCA* spectrum, Mathur et al. (2000) found evidence that PG 0946+341 is Compton-thick, but this again was based on assumptions that the underlying spectrum and normalization was that of a normal QSO since the counts were too few for detailed spectral fitting.
2. Mathur et al. (2001) analyzed an *ASCA* spectrum of the prototype BAL QSO PHL 5200 (with $z = 1.98$), wherein intrinsic absorption of $N_H^{intr} \sim 5 \times 10^{23}$ was required, covering 80% of the source. Intriguingly, the best-fit power-law photon index[4] in the 2–10 keV range ($\Gamma \sim 2.4$–2.8) for PHL 5200 is steeper than typical for non-BAL QSOs.
3. The simultaneous *ASCA*/*ROSAT* fitting of PG 1411+442 (Wang et al. 1999) shows a hard X-ray slope typical for non-BAL QSOs ($\Gamma \sim 2$; George et al. 2000; Reeves & Turner 2000), but there is also evidence for a strong, steep ($\Gamma = 3$) component of soft X-ray emission, in which non-BAL QSOs typically show $\Gamma \sim 2.5$. At $z = 0.09$, however, PG 1411+442 is the least luminous BAL QSO and suffers significant contamination from star-forming regions in its host galaxy.
4. Gallagher et al. (2001) found one BAL QSO, PG 2112+059 ($B = 15.5$, $z = 0.457$), which has perhaps the brightest flux of any BAL QSO. A best-fit power law of slope $\Gamma = 1.98^{+0.40}_{-0.27}$, partially ($97^{+3}_{-26}$%) covered by $1.0^{+1.4}_{-0.49} \times 10^{22}$ cm^{-2} of intrinsic absorption, suggests that this object could be a shrouded example of a typical QSO. However, while the object's "balnicity" index[5] of 2980 km s^{-1} seems to classify it firmly as a BAL QSO, the BALs are atypically shallow and the derived column rather low.

Further X-ray spectroscopy is critical to our basic understanding of BAL QSOs, but it is needed for some more typical objects and for as large a sample as is feasible. To begin to address this problem systematically, we performed a snapshot X-ray survey of BAL QSOs during Cycle 1 of the *Chandra X-Ray Observatory*. We describe below the chosen sample (§ 2) and their *Chandra* observations, ensemble spectral fitting (§ 3), X-ray brightness (§ 4), and the significance of our findings (§ 5). We summarize our findings in § 6 and present a brief discussion of individual objects in the sample in the Appendix.

2. SAMPLE AND OBSERVATIONS

We compiled a list of bona fide BAL QSOs with magnitudes (usually B or m_{pg}) brighter than 17. We derived expected count rates using the *Chandra* Portable Interactive Multimission Simulator, assuming that the intrinsic SED (before absorption) of BAL QSOs is similar to that of typical radio-quiet QSOs at similar luminosities. For the X-ray spectral photon index Γ, we used 2.5 in the soft X-ray

[4] The photon index Γ is related to the energy index α by $\alpha = \Gamma - 1$.

[5] Weymann et al. (1991) define the balnicity index by summing the equivalent width (in units of km s^{-1}) of any contiguous absorption that falls in the 3000–25,000 km s^{-1} range from the systemic redshift, if the absorption feature exceeds 2000 km s^{-1} in width and is at least 10% below the continuum level.

band (Schartel et al. 1996) and 1.8 above 2 keV (Lawson & Turner 1997). The power-law normalizations were derived from the observed optical magnitudes using values of α_{ox} typical for normal QSOs ($\alpha_{ox} = 1.6$; Green et al. 1995). We then calculated the absorbed *Chandra* broadband flux assuming an ($z = 0$) absorbing column of $N_H = 10^{22}$ cm^{-2}, which corresponds to an intrinsic column of $N_H^{intr} \sim 10^{23}$ cm^{-2} at typical sample redshifts. We thus calculated our proposed *Chandra* exposure times to result in a strong detection for each source.

The resulting sample spans a wide range of BAL QSO phenomena, including redshifts from 0.1 to 2.4, four dusty loBAL QSOs, two loBAL QSOs with metastable excited states of Fe II and Fe III (Hazard et al. 1987), a radio-moderate BAL QSO (Becker et al. 1997), and a gravitationally lensed BAL QSO. Table 1 lists the sample in order of increasing right ascension and includes mostly non–X-ray information.

All sources were observed between 1999 December 30 and 2000 May 15 using the back-illuminated S3 chip of the Advanced CCD Imaging Spectrometer (ACIS) on board *Chandra*. For the (optically) brightest object IRAS 07598+6508 ($B = 14.3$ mag), we used a subarray for more rapid readout to avoid the possible pileup of counts in ACIS. Table 2 lists the *Chandra* Observation ID (ObsID) and exposure times, observation dates, observed count rates, or 3 σ upper limits. The total exposure time for the sample of 10 objects is 36.2 ks. For each detected target, X-ray celestial coordinates matched optical counterpart coordinates to within $\sim 1''$ so that there is no ambiguity about identification.

3. DATA ANALYSIS AND SIMULTANEOUS SPECTRAL FITTING

We used reprocessed[6] data and extracted ACIS gain-corrected pulse-height invariant (PI) spectra from a 2.5 region around each QSO using the PSEXTRACT script

[6] CXCDS versions R4CU5UPD11.1 and higher, along with ACIS calibration data from the *Chandra* CALDB 2.0.

TABLE 1

SAMPLE PROPERTIES

Target	z	B[a] (mag)	N_H^{Gal} ($\times 10^{20}$cm^{-2})	BAL Ionization	Polarization (%)	References[b]	Comments[c]
Q0059−2735	1.595	18.0	1.97	Low	1.43 ± 0.16	1	Metastable Fe II and Fe III
Q0135−4001	1.850	17.3	1.97	High	...		
Q0254−334	1.863	17.8	2.26	High	0.0 ± 0.04	2	N V and O VI BALs
IRAS 07598+6508	0.148	14.3	4.34	Low	1.45 ± 0.14	3	*IRAS* and *ASCA* detection
FIRST J0840+3633.....	1.220	17.1	3.44	Low	4	4	Metastable Fe II and Fe III, Radio-moderate
Q0842+3431	2.120	17.5	3.41	High	0.55 ± 0.02	5	
UM 425	1.465	16.5	4.09	High	1.93 ± 0.17	2	Gravitational lens?, O VI BALs
LBQS 1235+1807B.....	0.449	16.9	1.96	Low	0.00 ± 0.07	1	*IRAS*
Q1246−0542	2.236	16.4	2.17	High	0.87 ± 0.07	2	*ROSAT* detection
SBSG 1542+541	2.371	16.8	1.27	High	...		Very high ionization

[a] The B_J magnitudes from USNOA-2.0 (Monet 1998) for all but UM 425 (Michalitsianos et al. 1997). Magnitudes are uncorrected for the BALs.
[b] The references are for polarization only.
[c] The references for comments can be found in the Appendix, where individual objects are discussed.
REFERENCES..—(1) Lamy & Hutsemekers 2000; (2) Hutsemekers et al. 1998; (3) Schmidt & Hines 1999; (4) Brotherton et al. 1997; (5) Ogle et al. 1999.

TABLE 2

SAMPLE OBSERVATIONS AND DERIVED PROPERTIES

Target	*Chandra* Observation ID	Time (ks)	Date of Observation	Counts	Count rate (counts ks^{-1})	log F_X (0.5–8 keV) Absorbed	log F_X (0.5–8 keV) Deabsorbed	log $L_{2\,keV}$	α_{ox}
Q0059−2735	813	4.39	2000 May 15	<5	<1.1	−14.19	−13.96	<26.13	>2.00
Q0135−4001	814	4.90	2000 Jan 2	23	4.7	−13.59	−13.29	26.94	1.84
Q0254−334[a]	815	2.43	2000 Jan 2	33	15.2	−12.96	−12.75	27.44	1.57
	135	1.04	2000 Feb 15	27	27.9				
IRAS 07598+6508	816	1.34	2000 Mar 21	10	6.7	−13.38	−13.19	24.73	2.34
FIRST J0840+3633.....	817	4.17	1999 Dec 30	8	1.9	−13.97	−13.85	25.98	2.11
Q0842+3431	818	4.09	2000 Jan 22	51	11.7	−13.17	−12.91	27.48	1.65
UM 425	819	2.61	2000 Apr 7	113	43.7	−12.53	−12.28	27.74	1.60
LBQS 1235+1807B.....	820	1.30	2000 Jan 21	<5	<3.8	−13.66	−13.43	<25.45	>2.01
Q1246−0542	821	5.41	2000 Feb 8	43	8.1	−13.34	−13.12	27.30	1.90
SBSG 1542+541	822	4.55	2000 Mar 22	78	19.7	−13.05	−12.79	27.64	1.73

NOTE.—Units of F_X and $L_{2\,keV}$ are ergs cm^{-2} s^{-1} and ergs s^{-1} Hz^{-1}, respectively. The deabsorbed flux values $L_{2\,keV}$ and α_{ox} are all calculated using our best-fit partial covering spectral model from Table 3, with the intrinsic (redshifted) absorption component removed from the best-fit model. We note that the use of the *absorbed* fluxes would decrease log L_X by about 0.23 and thereby increase α_{ox} by about 0.1.
[a] Fluxes and luminosities calculated from average count rate of the two *Chandra* observations.

TABLE 3

SPECTRAL FIT PARAMETERS

Model	Γ	$N_{\rm H}^{\rm intr}$ ($\times 10^{22}$ cm^{-2})	Covering Fraction	χ^2 (DOF)[a]
A.....	$1.08^{+0.13}_{-0.13}$	...	...	75.8 (62)
B.....	$1.44^{+0.23}_{-0.22}$	$1.6^{+0.9}_{-0.8}$	...	64.6 (61)
C.....	$1.80^{+0.35}_{-0.35}$	$6.5^{+4.5}_{-3.8}$	$0.80^{+0.09}_{-0.17}$	56.9 (60)

NOTE.—The fitted parameters are based on simultaneous fitting of unbinned spectra using Cash statistics. Uncertainties are 90% confidence limits. Models A fits a global power-law continuum of photon index Γ with individual neutral Galactic absorption of column $N_{\rm H}^{\rm Gal}$ (see Table 3); Model B includes global neutral absorption of column $N_{\rm H}^{\rm intr}$ at each quasar's redshift; Model C allows for a global partial covering fraction of the continuum by $N_{\rm H}^{\rm intr}$.

[a] The values of χ^2 are based on spectra binned to 5 counts bin^{-1} using given fitted parameters.

described in the standard thread for the *Chandra* Interactive Analysis of Observations (CIAO2.0). This script creates an aspect histogram file, and the response matrix and ancillary response[7] calibration files (RMFs and ARFs, respectively) appropriate to the source position on chip (which is time-dependent because of dither) and CCD temperature (-120 C). We extract background in PI space using an annulus extending typically from 5″ to 50″ around the source. In every case, the total background normalized to the source extraction area was less than 1 count, so we henceforth ignore background. In all analyses, we ignored channels below 0.5 keV since the ACIS response at lower energies is not well calibrated. Above 0.5 keV, the calibration is accurate to better than 10%. Channels above 6 keV were also ignored because of insufficient counts. Two final PI spectrum files were created for each source, one with no binning and one binned to a minimum of 5 counts bin^{-1}.

We perform spectral modeling for the six sources from Table 2 with more than 20 counts. We used SHERPA, a generalized modeling and fitting environment within CIAO2.0. Since each source spectrum taken individually has insufficient counts to usefully constrain the intrinsic absorption or power-law spectral index, instead we *simultaneously* fitted all six spectra. We fitted only the six BAL QSOs from Table 2 with more than 20 counts each. Note that these sources are all hiBAL QSOs, so the spectral parameters we derive may not apply to loBAL QSOs. We tested several source models, for which the best-fit values are recorded in Table 3.

Model A is simply a global power law with an individual flux normalization for each QSO and ($z = 0$) absorption fixed to the Galactic value for each QSO:

$$N(E) = A_i E^{-\Gamma} e^{-N_{H,i}^{\rm Gal}\sigma(E)} \text{ photons cm}^{-2}\text{ s}^{-1}\text{ keV}^{-1}\ .$$

In this formula, A_i is the normalization for the ith spectrum, but Γ is a *global* power-law emission component. $N_{{\rm H},\,i}$ is the equivalent Galactic neutral hydrogen column density that characterizes the effective absorption (by cold gas at solar abundance) for the ith source, with $\sigma(E)$ being the corresponding absorption cross section (Morrison & McCammon 1983). This simple fit yields an unusually flat continuum slope ($\Gamma = 1.08 \pm 0.13$), which is a signal that intrinsic absorption may be present. For determining the best-fit parameter values, we use Powell optimization with Cash statistics. This allows the use of unbinned spectral data, and we quote 90% confidence limits on fitted parameters in Table 3 and hereafter.

In Model B, we add a neutral absorber at the systemic redshift of each spectrum by multiplying Model A by a further term $e^{-N_{\rm H}^{\rm intr}\sigma[E(1+z_i)]}$. Here the key feature is that all the intrinsic column density parameters $N_{\rm H}^{\rm intr}$ are linked together, giving just a single free "intrinsic absorption" component. Similarly, the overall model amplitudes are free to vary individually, but again only one global power-law spectral index is fitted. The best-fit slope of Model B is $\Gamma = 1.44 \pm 0.23$, with intrinsic (rest-frame) absorption $N_{\rm H}^{\rm intr} = 6.5^{+4.5}_{-3.8} \times 10^{22}$ cm^{-2}.

We examined the relative quality of different model fits using χ^2 statistics, which must be performed on binned data. We binned the photon events to 5 counts bin^{-1} and estimate the variance using the background and source model amplitudes rather than the observed counts data (STATISTIC CHI MVAR in CIAO2.0). Table 3 presents the best-fit (Cash) model parameters together with their reduced χ^2 statistics. The results of χ^2 fitting confirm that the inclusion of a redshifted absorber (Model B) improves the fit at 99.7% (3 σ) confidence (using the F-test).

Inclusion of a *global* partial covering parameter C_f for the redshifted absorbers (Model C) substitutes the intrinsic absorption term in Model B with the expression

$$C_f e^{-N_H^{\rm intr}\sigma[E(1+z_i)]} + (1 - C_f)\ .$$

Here the last term in parentheses represents the fraction of light that escapes the source without absorption. Model C improves the fit, again at 99.5% confidence (F-test), relative to a redshifted absorber with no partial covering. The "composite" BAL QSO has intrinsic (rest-frame) absorption $N_{\rm H}^{\rm intr} = 6.5^{+4.5}_{-3.8} \times 10^{22}$ cm^{-2} covering 80^{+9}_{-17}% of the source, whose intrinsic power-law energy index $\Gamma = 1.80 \pm 0.35$.

In Figure 1, we present the summed *Chandra* X-ray spectrum for the six BAL QSOs with more than 20 counts. The sum of all the individual source models from the global best-fit Model C is overplotted, both with and without the absorber. The dashed line shows the "deabsorbed" model spectrum, where the intrinsic absorption component is removed from the best-fit model. Residuals for (similarly summed) models A, B, and C are also shown. We caution that this is essentially a composite of residuals from individual sources with different values of redshift and galactic absorption, and so features do not correspond directly to those expected in a single spectrum. However, the result is useful for visualization purposes since the redshifts for the spectral subsample—from 1.465 to 2.371, with mean $\bar{z} = 1.98 \pm 0.33$—happen not to range so widely as in the full sample. Neither is the counts-weighted redshift of 1.93 significantly different from this mean.

Figure 2 shows the confidence contours for Model C, in which it can be seen that the absorption is required at more than 2 σ confidence. The best-fit power-law index Γ for our BAL QSO sample is entirely consistent with the mean of $\sim 1.89 \pm 0.05$ with a dispersion of $\sigma = 0.27 \pm 0.04$ seen with *ASCA* for radio-quiet (RQ) QSOs at redshifts $z > 0.05$ (Reeves & Turner 2000). Measurements in a similar redshift

[7] RMFs are used to convert the ACIS pulse height (deposited charge) to energy. ARFs calibrate the effective collecting area of a specified source region on ACIS as a function of incident photon energy.

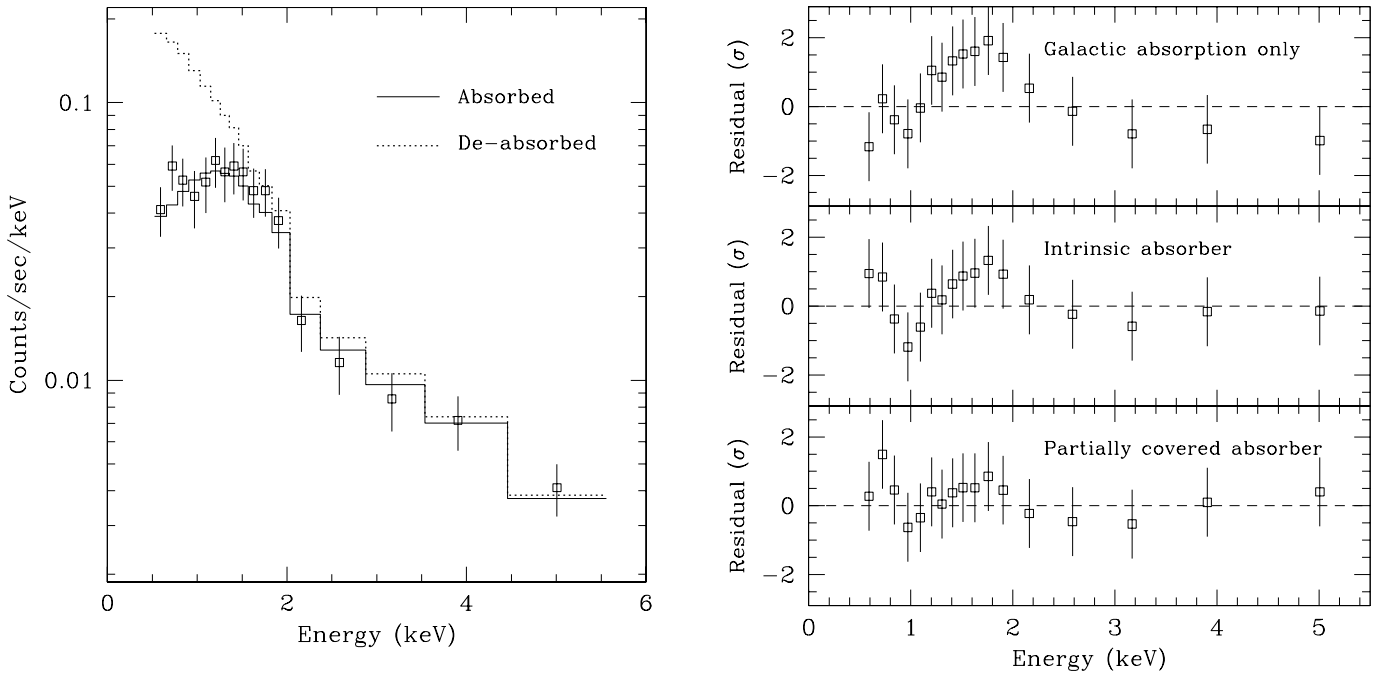

FIG. 1.—*Left*: Summed *Chandra* X-ray spectrum for the BAL QSOs with more than 20 counts. The sum of the all the individual source models is plotted over the merged event lists of all six objects. The solid line shows the global best-fit model (Model C in Table 3). The dashed line shows the "deabsorbed" model spectrum, in which the intrinsic absorption component is removed from Model C *after* fitting. *Right*: Residuals for models A, B, and C (Table 3 and § 3). These represent the overall sum of the residuals in the observed frame, so that remaining rest-frame features would appear blurred in this representation.

range are perhaps more relevant, so we compiled *ASCA* measurements from Reeves & Turner (2000) and Vignali et al. (1999) for all 10 of the $z > 1.3$ RQ QSOs with measured power-law energy indices. Redshifts for this comparison sample range from 1.3 to 3.0, with a mean of 2.1. The average index for the comparison sample is $\Gamma = 1.8$ with dispersion 0.15, which is indistinguishable from our results for the *Chandra* BAL QSO sample.

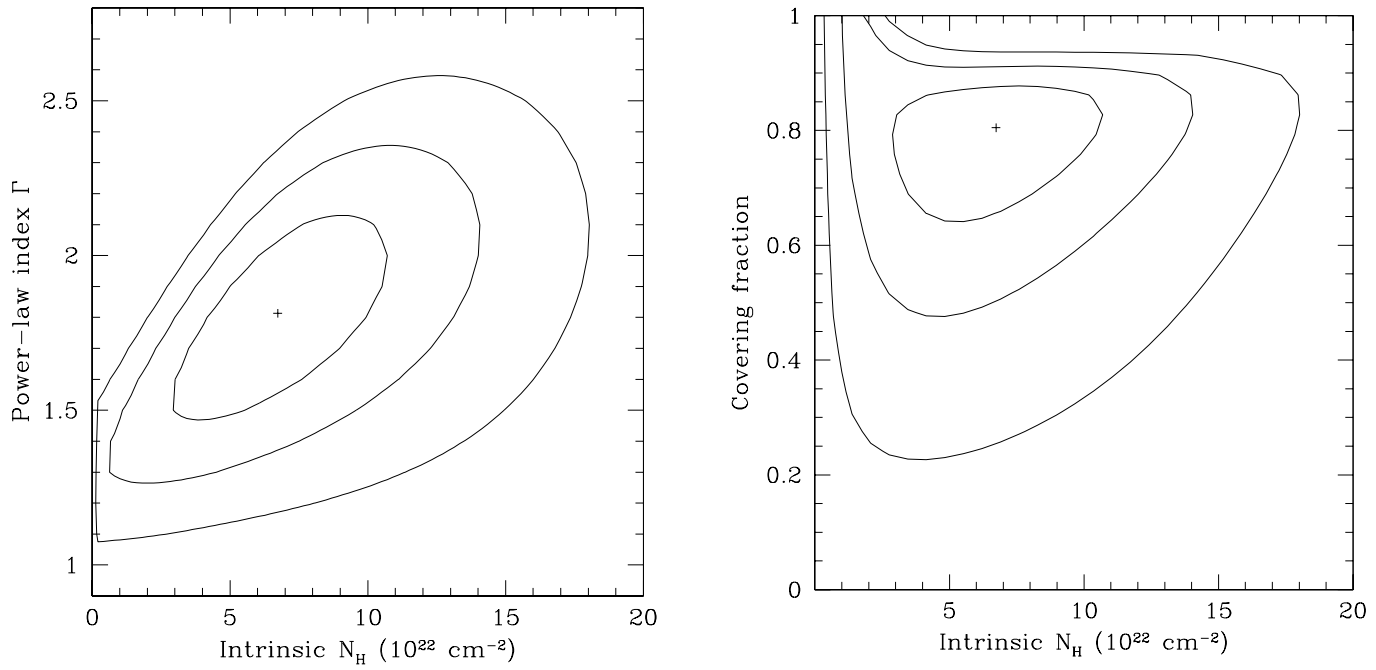

FIG. 2.—Joint (1, 2, and 3 σ) confidence intervals for spectral fit parameters for our simultaneous fit to the six *Chandra* BAL QSOs with more than 20 counts using Model C (Table 3 and § 3). *Left*: Redshifted intrinsic absorption and power-law spectral index Γ. *Right*: Confidence intervals for redshifted absorption and covering fraction.

The quality of the spectra are not sufficient to also constrain ionization or metallicity of the absorber, justifying the assumption of neutral absorbers with solar metallicity in our modeling. Modeling with either higher metallicities or with ionized absorbers would only increase the required intrinsic column in the best-fit models but is very unlikely to substantially change the power-law slope.

4. X-RAY BRIGHTNESS

Now that we have a *measured* mean spectral shape for hiBAL QSOs, for the first time we can calculate fluxes consistently using the best-fit model with the redshifted absorption component removed. This tells us what α_{ox} values BAL QSOs would have without their intrinsic absorption since their (deabsorbed) intrinsic SEDs are well characterized by the above slope. We use the best-fit composite X-ray spectral model to calculate the observed fluxes in the 0.5–8 keV band in Table 2. We derive the deabsorbed flux in the same band and use these to calculate the monochromatic rest-frame luminosities at 2 keV, also shown in Table 2. Optical magnitudes from Table 1 are used to derive the 2500 Å luminosities, and from these we calculated the optical–to–X-ray index α_{ox}. All luminosities are calculated assuming $H_0 = 50$ km s^{-1} Mpc^{-1} and $q_0 = 0.5$, with specific optical normalization from Marshall et al. (1984).

Using the deabsorbed fluxes from our full best-fit model in the observed *Chandra* band (0.5–8 keV) and also a consistent power-law slope $\Gamma = 1.8$ for the K-correction, the resulting α_{ox} values (or limits) range from 1.56 to 2.36, with a mean of 1.87. We note that use of the *absorbed* fluxes would decrease log L_X by about 0.23 and thereby increase α_{ox} by about 0.1.

We must be careful when we compare α_{ox} for our BAL QSO sample to previous results derived from observed fluxes in different (e.g., *ROSAT*) bandpasses or assuming different X-ray slopes. As a consistency check with previous results (e.g., GM96), we first simulate what would have been seen by *ROSAT*. To do this, we calculate with our full best-fit model the flux that would be observed in the *ROSAT* (0.5–2 keV) band. The resulting α_{ox} values range from 1.7 to 2.5, with a mean of 2.0, which is consistent with the *ROSAT* BAL QSO results for GM96 (most of which were nondetections).

Figure 3 shows the deabsorbed luminosities and α_{ox} for our sample relative to the composite points for large samples of radio-quiet QSOs observed by *ROSAT* (Green et al. 1995; Yuan et al. 1998). We caution that those *ROSAT* points are calculated in the *ROSAT* bandpass assuming a steeper slope $\Gamma = 2.5$, applicable to *ROSAT*-observed radio-quiet quasars. With the modeled intrinsic absorption removed, the hiBAL QSOs in our sample fit reasonably well along the empirical trend of increasing α_{ox} (weakening X-ray emission) with increasing L_{opt}. On the other hand, the four low-ionization BAL QSOs in our sample are extremely X-ray weak. Two are not detected at all (for which we assign 5 counts as an upper limit). Of the two loBAL QSOs that are detected, one is the most nearby object (at $z = 0.148$), and the other is a radio-intermediate BAL QSO.

5. DISCUSSION

Previous estimates of column densities in BAL QSO samples came by *assuming* that each BAL QSO had an intrinsic X-ray continuum of shape and normalization

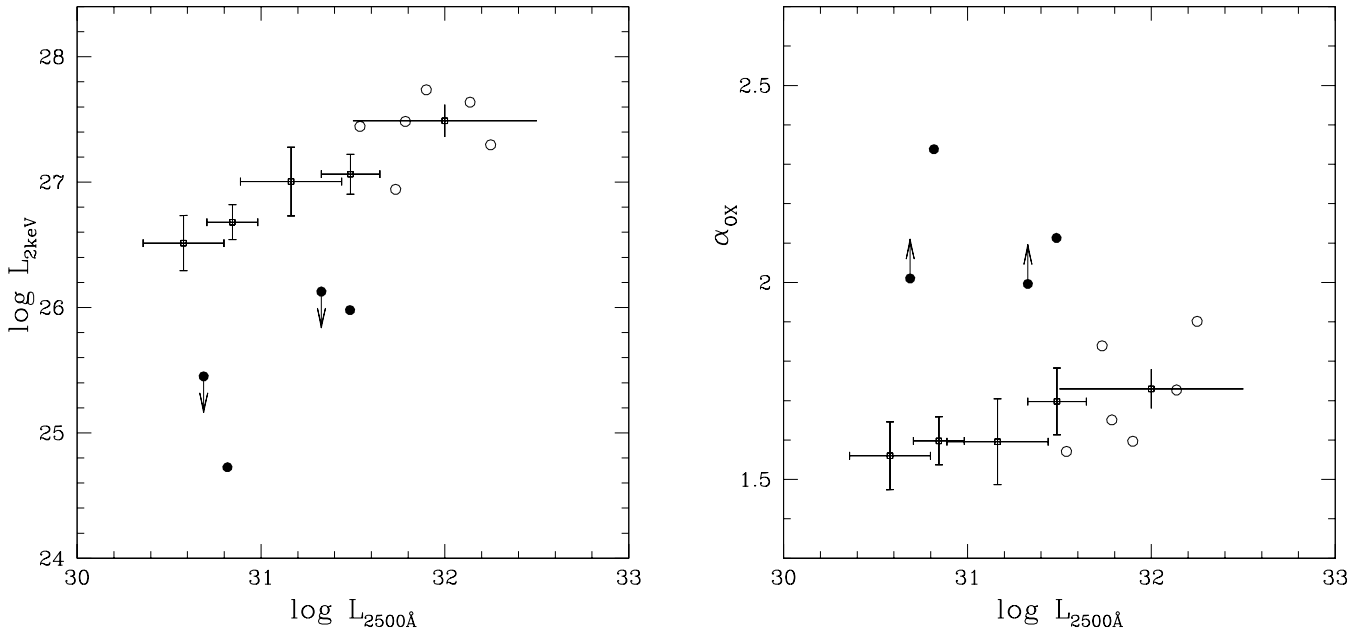

FIG. 3.—*Left*: The log of the monochromatic (2 keV) X-ray luminosity plotted against the log of monochromatic 2500 Å optical luminosity for quasars (both in units of ergs s^{-1} Hz^{-1}). *Right*: Optical–to–X-ray spectral slope α_{ox} (from 2500 Å to 2 keV), also plotted against log L_{2500}. In both panels, the circles depict the 10 BAL QSOs in our *Chandra* sample. The filled circles are those objects known to have loBALs. The X-ray luminosity and α_{ox} are deabsorbed, i.e., calculated without N_H^{intr} using our best-fit Model C. The arrows mark limits to X-ray luminosity in our *Chandra* exposures. The length of the arrow is used to illustrate the effect of using absorbed rather than deabsorbed fluxes in our calculations: log L_X would decrease by about 0.23 and thereby increase α_{ox} by about 0.1. The open squares with error bars are means from co-added subsamples of radio-quiet LBQS QSOs observed in the RASS (Green et al. 1995). The error bars are the rms dispersion of the QSOs in each bin. We also add one mean point at higher luminosity (log $L_{2500} > 31.5$) for *ROSAT*-observed radio-quiet QSOs from Yuan et al. (1998).

(relative to the optical) consistent with normal radio-quiet quasars (GM96; Gallagher et al. 1999). In most previous cases, the intrinsic absorbing column was estimated by simply scaling up $N_{\rm H}^{\rm intr}$ until the expected X-ray fluxes (predicted using B and $\alpha_{\rm ox}$) matched the observed fluxes or flux upper limits.

In the current study, we detect most of the BAL QSOs and now confirm via actual spectral fitting that the underlying continuum is consistent with that of normal radio-quiet QSOs. In the ensemble spectrum we also *detect* not only the predicted strong absorption but show the appropriateness of partial covering for the spectral model. Using the deabsorbed model, we now derive actual $\alpha_{\rm ox}$ values (rather than limits), with or without the intrinsic absorbing column included.

The best-fit power-law slope we find is harder than the slope of $\Gamma = 2.8 \pm 0.4$ derived for the bright loBAL QSO PHL 5200 by Mathur et al. (2001) using a 90% covering fraction. Intriguingly, however, their inclusion of a high-energy (18 keV) cutoff in the model yields the best overall fit that they find and a slope of 2.4 ± 0.4, which is consistent with the current result within the errors. However, PHL 5200 may be a special case. With $\alpha_{\rm ox} = 1.5$, PHL 5200 is the X-ray brightest BAL QSO ever observed, and its polarization is also quite high (5% at λ5500; Schmidt & Hines 1999). To account for its X-ray brightness requires far more than the simple application of an additional 10% of reflected X-rays since PHL 5200 is an order of magnitude brighter in X-rays than most BAL QSOs.

The BAL clouds along our sight line may be diaphanous, shredded, or otherwise holey, affecting the measured partial covering fraction. However, the measured fraction is likely decreased by X-ray emission reflected toward us by clouds having a direct line of sight to the nucleus. Such reflection should be associated with increased polarization, but polarization measurements for six of the objects in our sample show no correlation with $F_{\rm X}$, $L_{\rm X}$, or $\alpha_{\rm ox}$.

5.1. *Low-Ionization BAL QSOs*

Only about 1% of optically selected QSOs show broad absorption in lower ionization lines of Mg II or Fe II. By contrast, Boroson & Meyers (1992) found that loBAL QSOs constitute 10% of IR-selected quasars. LoBAL QSOs are reddened (Sprayberry & Foltz 1992; Egami et al. 1996) and tend to have particularly high polarization (Schmidt & Hines 1999). We have included four loBAL QSOs in our *Chandra* sample. Since insufficient counts are available from the loBALs, the spectral model we adopt is from hiBAL QSOs only. This also means that the deabsorption applied to the X-ray fluxes of the loBALs probably underestimates their true column, causing even the deabsorbed $L_{\rm X}$ and $\alpha_{\rm ox}$ values in Table 2 and Figure 3 for these objects to look particularly X-ray weak.

We can interpret the difference between the $\alpha_{\rm ox}$ values for loBAL QSOs plotted in Figure 3 and a deabsorbed $\alpha_{\rm ox}$ of 1.7 (the mean value for the hiBAL QSOs alone) to be due to additional absorption in loBALs that is unaccounted for in our spectral model. The minimum difference is $\Delta\alpha_{\rm ox} \sim 0.3$, based on the lower limits to $\alpha_{\rm ox}$ of the undetected loBAL QSOs. Even neglecting any optical extinction, this corresponds to additional quenching of $L_{2\ {\rm keV}}$ of at least a factor of 6. Assuming that the same ($\Gamma = 1.80$) intrinsic power law applies to all BAL QSOs, we can infer that loBAL QSOs are shrouded by, at minimum, an additional intrinsic column of nearly 10^{23}–10^{24} cm^{-2} beyond that of the hiBAL QSOs. LoBAL QSOs may also have intrinsically steeper spectra so that their X-rays are more easily absorbed.

Even more rare than loBALs in optical surveys are the "iron loBALs," which exhibit absorption lines from metastable excited levels of Fe II. There are just a few iron loBAL QSOs known to date: Q0059−2735, FIRST J0840+3633, J1556+3517 (Becker et al. 1997), and Hawaii 167 (Cowie et al. 1994). Becker et al. (1997) noted a trend of radio power increasing with reddening and proposed that, as loBALs become more extinguished optically, their radio power increases, making iron loBAL QSOs a special radio-intermediate population of BAL QSOs. Sensitive radio surveys may thus uncover many more iron loBAL QSOs. We have observed two of the known iron loBAL QSOs, Q0059−2735 and FIRST J0840+3633. Both are quite weak in X-rays, the former not being detected at all. This indicates that iron loBALs, if they are indeed QSOs, may be nearly Compton-thick ($N_{\rm H}^{\rm intr} \geq 10^{24}$ cm^{-2}), thus beyond the reach of most X-ray surveys except perhaps at high redshift, where their observed-frame X-rays correspond to more penetrating hard X-ray emission in the quasar rest frame.

The decrease in polarization toward longer wavelengths in some loBALs suggests edge-on dust-scattering models (Kartje 1995) in which the scattered line of sight is less reddened, so that loBAL QSOs have been proposed as the *most* edge-on QSOs (Brotherton et al. 1997). On the other hand, loBAL QSOs may be nascent QSOs embedded in a dense, dusty star formation region (see, e.g., Voit, Weymann, & Korista 1993). The expected strong extinction has been seen (Sprayberry & Foltz 1992; Boroson & Meyers 1992) and could explain their low (1%–2%) incidence in optically selected samples. Luminous infrared galaxies such as IRAS 07598+6508 may have both nuclear starbursts and active nuclei fueled by large masses of gas and dust within a few hundred parsecs of the nucleus arising from mergers and viscous accretion (Canalizo & Stockton 2000). Nearby examples such as this object may be accessible analogs of high-redshift galaxies seen in their peak epoch of formation and growth (Scoville 1999).

Based only on their observed X-ray luminosities, an alternative to absorption is that loBAL QSOs may contain at best very weak active galactic nuclei (AGN) and are instead dominated by massive starbursts (see, e.g., Risaliti et al. 2000). The brightest nearby spiral galaxies observed by Fabbiano & Trinchieri (1985) show $\log L_{2\ {\rm keV}} = 23.5$, and elliptical galaxies achieve $\log L_{2\ {\rm keV}} = 24$, which is near to the apparent X-ray luminosity of our 2 detected loBAL QSOs. The nearby starburst galaxy NGC 3256 is driving a "superwind" (Moran, Lehnert, & Helfand 1999) and achieves $\log L_{2{\rm keV}} \sim 24.6$, which is similar to that of the loBAL QSO IRAS 07598+6508 in the current sample. However, the optical/UV emission and absorption-line properties of loBAL QSOs clearly indicate velocities far higher than achievable even by starburst superwinds (Leitherer, Robert, & Drissen 1992).

5.2. *Orientation, Evolution, and Outburst*

An alternative to the orientation hypothesis, in which every QSO has BAL clouds visible only along a privileged line of sight, is that BAL QSOs are in a phase of high accretion rate. If so, in analogy to narrow-line Seyfert 1 galaxies, we expect the intrinsic power law to be significantly steeper than normal QSOs (Mathur 2000; Brandt &

Gallagher 2000). The underlying power law that we detect in the current study does not favor such an interpretation. On the other hand, some counterexamples of steep X-ray spectrum BAL QSOs may exist (PHL 5200, Mathur et al. 2000; PG 1411+442, Wang et al. 1999).

In the orientation interpretation of the BAL phenomenon, $\sim$10% of QSOs show BALs because the overall BAL covering factor is $\sim$10%. The recent discovery of radio-selected BAL QSOs with both compact and extended radio morphologies and with both steep and flat spectra is inconsistent with a simple unified orientation scheme, which predicts only steep-spectrum sources for an edge-on geometry. Predominantly compact radio morphology and steep radio spectra in radio-selected BAL QSOs are reminiscent of compact steep spectrum quasars. These have been interpreted as young radio objects that are confined to a small region by dense gas but which later evolve extended radio lobes as they escape confinement (O'Dea 1998), which is analogous to the evolutionary model of BAL QSOs as young quasars emerging from cocoons (Voit et al. 1993). Rather than directly interpreting the fraction of QSOs with BALs as a covering factor, the observed fraction may instead reflect the portion of a QSO lifetime with strong outflows at large covering factor. If, in addition, mergers and interactions that trigger growth and accretion occur more frequently at early epochs, as expected, then an evolutionary trend is predicted; BAL QSOs should be more common at high redshifts. If a large, relatively unbiased sample of BAL QSOs can be accumulated, both evolution and orientation may need to be invoked to explain the observed population.

A recent tally (Chartas 2000) of QSOs has shown that 35% of gravitationally lensed QSOs show BALs, which is more than 3 times the rate in flux-limited optical QSO surveys. While the fraction of BAL QSOs may increase with look-back time, another viable explanation is that lensing magnification overcomes attenuation of the BAL QSO optical emission such that presently available flux-limited surveys of BAL quasars detect more gravitationally lensed BAL QSOs. Gray attenuation of a factor of about 5, as is also suggested by Goodrich (1997) from polarization observations of BAL QSOs, together with plausible average lensing magnification factors of $\sim$10 successfully reproduce the observations. The resulting prediction that the fraction of BAL QSOs should increase with survey sensitivity (see also Krolik & Voit 1998) seems to be borne out by the fact that at least three of five of the $z \geq 5$ QSOs found so far in the Sloan Digital Sky Survey show BALs (Zheng et al. 2000). However, these (small-sample) statistics could support either a lensing or an evolutionary model.

Increasingly, low-energy X-ray absorption is being reported in quasars at high redshift (Yuan et al. 2000; Fiore et al. 1998; Elvis et al. 1994). At this writing, the QSO with the highest known redshift (Sloan Digital Sky Survey J104433.04−012402.2 at $z = 5.8$; Brandt et al. 2001) is also X-ray weak ($\alpha_{ox} = 1.9$). BAL QSOs and similar absorbed AGNs may provide a significantly larger fraction of the cosmic X-ray background (CXRB) than would be estimated from their contribution to typical optically selected samples. Furthermore, as the simplest model fits demonstrate (Table 3), low signal-to-noise ratio (S/N) absorbed X-ray spectra of BAL QSOs will look hard ($\Gamma \leq 1.4$), like the CXRB spectrum. The apparently high fraction and nature of obscured faint sources with hard X-ray spectra reported in early deep *Chandra* fields (see, e.g., Giacconi et al. 2001; Hornschemeier et al. 2000) is being hotly debated but may contain many such objects. Our results provide a caution to interpretations of the spectra of these faint hard X-ray sources. Distant obscured quasars detected with very few counts may appear to be hard enough to compose much of the CXRB, while their true continuua could taper off more quickly at higher energies. Table 3 shows that partial covering can also strongly affect the apparent continuum slope even when absorption is detected. Extremely deep pointings may find a small number of such objects bright enough so that better X-ray spectral constraints are available. Samples of high-redshift and/or optically reddened objects from larger areas should be amassed at brighter fluxes by serendipitous surveys with wider sky coverage like the *Chandra* Multiwavelength Project (Green et al. 1999; Wilkes et al. 2001). Stacking or simultaneous fitting of X-ray spectra as performed here could help establish the detailed spectral characteristics and evolution of X-ray absorption in quasars.

6. SUMMARY

We have carried out a short-exposure *Chandra* survey of a sample of 10 bright BAL QSOs, with exposures ranging in length from 1.3 to 5.4 ks. Eight of the 10 sources are detected, with observed counts ranging from 8 to 113. Corresponding fluxes are rewardingly bright in the *Chandra* (0.5–8 keV) bandpass, ranging from 3×10^{-13} to 3×10^{-14} ergs cm^{-2} s^{-1}.

Simultaneous fitting of spectra from six BAL QSOs detected by *Chandra* shows that the "composite" BAL QSO has an underlying power-law spectral index $\Gamma = 1.80^{+0.35}_{-0.35}$ that is 80^{+9}_{-17}% covered by an intrinsic absorber of column $N_H = 6.50^{+4.5}_{-3.8} \times 10^{22}$ cm^{-2}. Our X-ray spectral constraints should represent those of an average hiBAL QSO. We note that the best-fit absorption column (with partial covering) of $\sim 6.5 \times 10^{22}$ cm^{-2} is far higher than would be naively measured from UV spectra from BAL equivalent widths or by direct conversion of residual intensity to optical depth, robustly confirming earlier suggestions. Truly high S/N X-ray spectra of typical BAL QSOs are still coveted since the cloud properties can then be studied in detail and compared to spectral information from the BALs in the rest-frame UV. Scattering modelscan, in principle, be tested with soft X-ray polarization measurements.

For the detected QSOs, the deabsorbed optical–to–X-ray spectral slope (α_{ox} from 2500 Å to 2 keV) varies from 1.6 to 2.3. The high-ionization BAL QSOs in our sample have deabsorbed values of α_{ox} consistent with those measured in optically selected radio-quiet QSOs of similar luminosity. The low-ionization BAL QSOs in our sample are X-ray weak, even after correcting for the composite intrinsic absorption. One explanation is that the absorbing column in these objects is substantially higher, but further investigation is of great interest, especially given the possible links of these objects to ultraluminous IR galaxies and mergers.

The authors would like thank Aneta Siemiginowska for her expert help with SHERPA as well as the entire *Chandra* team for making possible these very sensitive observations. This work was supported by *Chandra* grant GO 0-1030X and NASA grant NAS 8-39073.

APPENDIX A

INDIVIDUAL OBJECTS

Q0059−2735.—This strong loBAL was not detected by *Chandra*. It is highly reddened (Egami et al. 1996) and significantly polarized ($P = 1.60\% \pm 0.29\%$; Hutsemekers, Lamy, & Remy 1998). Although several examples now exist (Becker et al. 1997; Brotherton et al. 1997), Q0059−2735 is the prototypical iron loBAL, showing striking absorption lines in metastable iron (Hazard et al. 1987). The spectra of these objects are spectacular and completely dominated by their absorption features in the rest-frame UV.

Q0135−4001.—This object has normal, strong hiBALs (Korista et al. 1992).

Q0254−334.—Amongst our sample, this object is intrinsically brightest in X-rays and is not polarized ($P = 0.0 \pm 0.04$; Hutsemekers et al. 1998), implying that little of the observed emission is reflected into our line of sight. The rest-frame UV spectrum (Wright et al. 1982) has strong hiBALs, with no evidence for loBALs. We note that the count rates between the two observations differ at the 2.2 σ level, offering intriguing evidence for absorber variability, rarely if ever seen in high-luminosity BAL QSOs.

In our ACIS-S image, we also detect the $B = 17$ radio quasar PKS 0254−334 (PMN J0256−3315), which is 60″ distant and at a similar redshift (1.913). With 25 counts in ObsID 135 and 51 counts in ObsID 815, we derive a count rate of 0.022. Assuming $\Gamma = 1.6$, which is typical for radio-loud quasars (Reeves & Turner 2000), we derive an (absorbed) flux f(0.5–8 keV) $= 1.4 \times 10^{-13}$ ergs cm^{-2} s^{-1} [or f(0.5–2 keV) $= 4.1 \times 10^{-14}$ ergs cm^{-2} s^{-1}]. The (unabsorbed) X-ray luminosity $\log L_{2\,\mathrm{keV}} = 27.41$, which together with the USNO A2.0 magnitude $B = 18.4$ mag (Monet 1998), yields $\alpha_{ox} = 1.50$. As expected, this object is more X-ray bright than most radio-quiet quasars and significantly more so than most BAL QSOs.

IRAS 07598+6508.—Of the entire *Chandra* BAL QSO sample, this *IRAS*-selected loBAL shows the weakest observed X-ray emission relative to optical ($\alpha_{ox} = 2.36$), which is consistent with both the *ROSAT* upper limit from an 8.3 ks PSPC observation (GM96 and Gallagher et al. 1999), in which the object is detected only in the hard-sensitive *ASCA* Gas Imaging Spectrometer in a 40 ks observation. We owe our detection here in just 1.3 ks to *Chandra*'s tiny point-spread function (<1″ on-axis) and to the object's low redshift (0.148), perhaps abetted by some reflected X-ray emission implied by the object's significant optical polarization ($P = 1.5 \pm 0.1$; Schmidt & Hines 1999). Objects such as this may also have an appreciable contribution from a circumnuclear starburst in the X-ray bandpass (Lawrence et al. 1997).

While most optically selected quasars fall in a narrow range of L(FIR)/L_{opt} (Andreani, Franceschini, & Granato 1999), IRAS 07598+6508 is *IRAS*-selected and has a ratio about an order of magnitude larger than the mean. In the unified AGN scheme, L(FIR)/L_{opt} may be related to the viewing angle of the torus, with more inclined objects having larger values. If BAL QSOs are seen at a line of sight that skims outflowing BAL clouds ablated from a disk, the likelihood that the disk and torus tend to be aligned means that BAL QSOs, and the reddened loBALs in particular, are probably severely underrepresented in optical surveys.

FIRST J0840+3633.—This iron loBAL is one of many BAL QSOs selected by the FIRST radio survey (Becker et al. 2000). While quite X-ray weak ($\alpha_{ox} = 2.2$) and at higher redshift than the other iron loBAL in our sample (IRAS 07598+6508), FIRST J0840+3633 is detected in our survey. Some of the detected X-ray emission may be reflected, as suggested by the very significant polarization in this object ($P = 4\%$ at the 2000 Å rest frame; Brotherton et al. 1997).

Q0842+3431 (CSO 203).—This hiBAL QSO has low polarization ($P = 0.55\% \pm 0.02\%$; Ogle et al. 1999) and appears to have X-ray brightness typical for a non-BAL of its optical luminosity.

UM 425 (Q1120+019).—This hiBAL QSO has the highest X-ray flux in our sample and also has high polarization ($P = 1.93\% \pm 0.17\%$; Hutsemekers et al. 1998). Two quasars at identical redshifts are seen, separated by 6.″5 and about 4.5 mag in optical brightness. UM 425A and UM 425B may well be lensed, especially since both spectra show BALs (Meylan & Djorgovski 1989). It could also be an intriguing case of merger-triggered AGNs (Kochanek, Falco, & Munoz 1999) interacting within their 60–100 kpc separation. UM 425B is expected to show only about 1 or 2 counts in our 2.6 ks exposure, and consistent with that, it is not detected.

LBQS 1235+1807B (IRAS F12358+1807).—We would certainly have expected to detect this optically bright, low-redshift object in our *Chandra* exposure if it were a non-BAL or even a hiBAL QSO. However, it is an *IRAS*-detected loBAL, with little expectation of reflected nuclear emission since it is unpolarized in the optical ($P = 0.0\% \pm 0.07\%$; Lamy & Hutsemeker 2000).

Q1246−0542.—It is notable that this BAL QSO is particularly X-ray weak for a hiBAL QSO ($\alpha_{ox} = 1.9$) and may show weak evidence for an Mg II BAL (Hutsemekers et al. 1998). A high S/N spectrum reaching Mg II at 9200 Å would be valuable. Intriguingly, polarization may be variable in this object: Schmidt & Hines (1999) report $P = 2.0\% \pm 0.3\%$, while Hutsemekers et al. (1998) list $P = 0.87\%$. If a substantial fraction of the detected X-rays are scattered into our line of sight, then this implies that the observed X-ray flux should also vary. We see no significant variability within the short timescale of our 5.4 ks *Chandra* observation. Our derived flux is also consistent with that seen by GM96 with *ROSAT*.

SBSG 1542+541.—This bright high-redshift hiBAL QSO has very highly ionized BALs (including O VI, Ne VIII, and Si XII; Telfer et al. 1998) and appears to have an X-ray brightness typical for a non-BAL of its optical luminosity.

REFERENCES

Andreani, P., Franceschini, A., & Granato, G. 1999, MNRAS, 306, 161
Arav, N., Korista, K. T., de Kool, M., Junkkarinen, V. T., & Begelman, M. C. 1999, ApJ, 516, 27
Becker, R. H., Gregg, M. D., Hook, I. M., McMahon, R. G., White, R. L., & Helfand, D. J. 1997, ApJ, 479, L93
Becker, R. H., White, R. L., Gregg, M. D., Brotherton, M. S., Laurent-Mühleisen, S. A., & Arav, N. 2000, ApJ, 538, 72
Boroson, T. A., & Meyers, K. A. 1992, ApJ, 397, 442
Brandt, W. N., & Gallagher, S. C. 2000, NewA Rev., 44, 461
Brandt, W. N., Guainazzi, M., Kaspi, S., Fan, X., Schneider, D. P., Strauss, M. A., Clavel, J., & Gunn, J. E. 2001, AJ, 121, 591
Brotherton, M. S., Tran, H. D., Van Breugel, W., Dey, A., & Antonucci, R. 1997, ApJ, 487, L113
Canalizo, G., & Stockton, A. 2000, AJ, 120, 1750

Chartas, G. 2000, ApJ, 531, 81
Cowie, L. L., et al. 1994, ApJ, 432, L83
de Kool, M., & Begelman, M. C. 1995, ApJ, 455, 448
Egami, E., Iwamuro, F., Maihara, T., Oya, S., & Cowie, L. L. 1996, AJ, 112, 73
Elvis, M. 2000, ApJ, 545, 63
Elvis, M., Fiore, F., Wilkes, B., McDowell, J., & Bechtold, J. 1994, ApJ, 422, 60
Fabbiano, G., & Trinchieri, G. 1985, ApJ, 296, 430
Fabian A. 1999, MNRAS, 308, L39
Fiore, F., Elvis, M., Giommi, P., & Padovani, P. 1998, ApJ, 492, 79
Gallagher, S. C., Brandt, W. N., Laor, A., Elvis, M., Mathur, S., Wills, B. J., & Iyomoto, N. 2001, ApJ, 546, 795
Gallagher, S. C., Brandt, W. N., Sambruna, R. M., Mathur, S., & Yamasaki, N. 1999, ApJ, 519, 549
George, I. M., Turner, T. J., Yaqoob, T., Netzer, H., Laor, A., Mushotzky, R. F., Nandra, K., & Takahashi, T. 2000, ApJ, 531, 52
Giacconi, R., et al. 2001, ApJ, 551, 624
Goodrich, R. W. 1997, ApJ, 474, 606
Green, P. J., & Mathur, S. 1996, ApJ, 462, 637 (GM96)
Green, P. J., et al. 1995, ApJ, 450, 51
———. 1999, BAAS, 195, 8008
Hamann, F. 1998, ApJ, 500, 798
Hamann, F., Korista, K. T., & Morris, S. L. 1993, ApJ, 415, 541
Hazard, C., McMahon, R. G., Webb, J. K., & Morton, D. C. 1987, ApJ, 323, 263
Hornschemeier, A. E., et al. 2000, ApJ, 541, 49
Hutsemekers, D., Lamy, H., & Remy, M. 1998, A&A, 340, 371
Kartje, J. F. 1995, ApJ, 452, 565
Kochanek, C. S., Falco, E. E., & Munoz, J. A. 1999, ApJ, 510, 590
Korista, K. T., et al. 1992, ApJ, 401, 529
Krolik, J. H., & Voit, G. M. 1998, ApJ, 497, L5
Lamy, H., & Hutsemekers, D. 2000, A&AS, 142, 451
Lawrence, A., Elvis, M., Wilkes, B. J., McHardy, I., & Brandt, N. 1997, MNRAS, 285, 879
Lawson, A. J., & Turner, M. J. L. 1997, MNRAS, 288, 920
Leighly, K. M. 1999, ApJS, 125, 317
Leitherer, C., Robert, C., & Drissen, L. 1992, ApJ, 401, 596
Marshall, H. L., Avni, Y., Braccesi, A., Huchra, J. P., Tananbaum, H., Zamorani, G., & Zitelli, V. 1984, ApJ, 283, 50
Mathur S. 2000, MNRAS, 314, L17
Mathur S., et al. 2000, ApJ, 533, L79
Mathur, S., Matt, G., Green, P. J., Elvis, M., & Singh, K. P. 2001, ApJ, 551, L13
Mathur, S., Wilkes, B. J., Elvis, M., & Fiore, F. 1994, ApJ, 434, 493
Meylan, G., & Djorgovski, S. 1989, ApJ, 338, L1
Michalitsianos, A. G., Falco, E. E., Munoz, J. A., & Kazanas, D. 1997, ApJ, 487, L117
Monet, D. G. 1998, BAAS, 1931, 2003
Moran, E. C., Lehnert, M. D., & Helfand, D. J. 1999, ApJ, 526, 649
Morrison, R., & McCammon, D. 1983, ApJ, 270, 119
Murray, N., & Chiang, J. 1995, ApJ, 454, L105
O'Dea, C. P. 1998, PASP, 110, 493
Ogle, P. M., Cohen, M. H., Miller, J. S., Tran, H. D., Goodrich, R. W., & Martel, A. R. 1999, ApJS, 125, 1
Pounds, K. A., Done, C., & Osborne, J. P. 1995, MNRAS, 277, L5
Reeves, J. N., & Turner, M. J. L. 2000, MNRAS, 316, 234
Risaliti, G., Gilli, R., Maiolino, R., & Salvati, M. 2000, A&A, 357, 13
Schartel, N., et al. 1996, MNRAS, 283, 1015
Scoville, N. 1999, Ap&SS, 269, 367
Schmidt, G., & Hines, D. 1999, ApJ, 512, 125
Sprayberry, D., & Foltz, C. B. 1992, ApJ, 390, 39
Telfer, R. C., Kriss, G. A., Zheng, W., Davidsen, A. F., & Green, R. F. 1998, ApJ, 509, 132
Vignali, C., Comastri, A., Cappi, M., Palumbo, G. G. C., Matsuoka, M., & Kubo, H. 1999, ApJ, 516, 582
Voit, G. M., Weymann, R. J., & Korista, K. T. 1993, ApJ, 413, 95
Wang, T. G., Wang, J. X., Brinkmann, W., & Matsuoka, M. 1999, ApJ, 519, L35
Weymann, R. J., Morris, S., L., Foltz, C. B., & Hewett, P. C. 1991, ApJ, 373, 23
Wilkes, B. J., et al. 2001, in ASP Conf. Ser. 232, New Era of Wide Field Astronomy, ed. R. G. Clowes, A. J. Adamson, & G. E. Bromage (San Francisco: ASP), in press
Wright, A. E., Morton, D. C., Peterson, B. A., & Jauncey, D. L. 1982, MNRAS, 199, 81
Yuan, W., Brinkmann, W., Siebert, J., & Voges, W. 1998, A&A, 330, 108
Yuan, W., Matsuoka, M., Wang, T., Ueno, S., Kubo, H., & Mihara, T. 2000, ApJ, 545, 625
Zheng, W., et al. 2000, AJ, 120, 1607